

LASER APPLICATIONS AND OTHER TOPICS IN QUANTUM ELECTRONICS

PACS numbers: 42.81.Pa
DOI: 10.1070/QE2006v036n03ABEH013136

Use of Spun optical fibres in current sensors

V.P. Gubin, V.A. Isaev, S.K. Morshnev, A.I. Sazonov,
N.I. Starostin, Yu.K. Chamorovskii, A.I. Usov

Abstract. **The polarisation properties of a Spun optical fibre are studied in connection with their applications in fibreoptic current sensors based on the Faraday effect. A model of this fibre is proposed which represents it as an anisotropic medium with the spiral structure of the fast and slow birefringence axes. A sensor is developed based on an all-fibre low-coherence linear interferometer with a threshold sensitivity of 70 mA Hz$^{-1/2}$, a maximum measured current of 3000 A, and a scale-factor reproducibility of $\pm 0.6\%$. It is found that for a given diameter of the fibre contour, the normalised sensitivity is independent of the fibre length. The experimental results confirm the theory.**

Keywords: *optical fibre, Faraday effect, current sensor*.

1. Introduction

Unremitting interest in fibreoptic current sensors (FOCSs) based on the Faraday effect in an optical fibre [1 – 3] is explained by considerable promising possibilities of these devices. The natural decoupling from the line voltage, the absence of interferences, a fast response and high measurement accuracy, a small size and a small weight – this is by no means a complete list of the advantages of FOCSs over conventional current sensors.

Standard optical fibres used in communication lines cannot be applied in the sensitive elements of FOCSs because of their internal birefringence, which is random along the fibre length both in the magnitude and direction of its axes. At present, different types of special fibres are used in FOCSs, for example, fibres with low birefringence (of the LoBi type). In this case, the linear birefringence induced by the elastic bending of a fibre is compensated either by elastic twisting around the fibre axis [4] or by annealing the sensitive element at a high temperature after it winding [3]. Optical fibres of the Spun type, which are manufactured by drawing a fibre from a rotating preform having a high internal linear birefringence, are also quite promising [1].

V.P. Gubin, V.A. Isaev, S.K. Morshnev, A.I. Sazonov, N.I. Starostin, Yu.K. Chamorovskii, A.I. Usov Institute of Radio Engineering and Electronics, Russian Academy of Sciences, pl. Vvedenskogo, 141190 Fryazino, Moscow region, Russia; e-mail: nis229@ire216.msk.su

Received 8 September 2005
Kvantovaya Elektronika **36** (3) 287 – 291 (2006)
Translated by M.N. Sapozhnikov

Spun fibres have been already used for about 15 years [1, 5, 6]; however, their properties and mechanisms restricting their applications have not been treated unambiguously so far. In particular, there exist important disagreements in the methods and even ideology of interpretation of the results obtained [1, 6].

The preform for a Spun fibre is similar to that for a fibre with a strong linear birefringence (of the HiBi type); however, it is rotated during fibre drawing, which results in the monotonic turning of glass layers with respect to each other in the region of the preform-material softening in the plane perpendicular to the fibre axis. It is reasonable to assume that the fast and slow axes of the linear internal birefringence are 'frozen' during fibre drawing in the form of a spiral with a step determined by the rotation period of the preform and the drawing rate. Unlike [1], elastic tensions inducing a noticeable circular birefringence are not 'frozen' upon drawing. For example, LoBi fibres, manufactured by using a similar technology, do not exhibit circular birefringence [7, 8] in the presence of a spiral structure.

In this paper, we analyse the properties of Spun fibres from the point of view of their application in FOCSs based on the formalism of the differential Jones matrix by treating the fibre as an anisotropic medium with the spiral structure of the fast and slow linear birefringence axes. We explained earlier [7] some properties of LoBi fibres with weak birefringence by the existence of this structure. Note that in papers [1, 9] the Spun fibre was analysed without the use of differential matrices, whereas in [6] the results were interpreted by using the differential matrix on the basis of linear polarisations. We studied experimentally the applicability of Spun fibres as sensitive elements in FOCSs and obtained the results confirming the validity of our model.

We used the approach based on the fact that orthogonal circularly polarised light waves propagating along a silica fibre in a longitudinal magnetic field acquire the Faraday phase shift. This shift is equal to $\Delta\varphi_F = 2VB_zL$, where V is the Verdet constant for the fibre core material; B_z is the longitudinal component of the magnetic field; and L is the fibre length. If the optical fibre forms a closed coil inside which a conductor with a current flowing in it is placed, then $\Delta\varphi_F = 2VN_0J$, where N_0 is the number of coils and J is the current flowing through the conductor. The theory considered below allows us to calculate the Faraday phase shift $\Delta\varphi_F$ taking into account the basic types of birefringence existing in a real Spun fibre and to compare the results of calculations with experimental data.

2. Theory

The polarisation properties of radiation propagating in a Spun fibre with the spiral structure of the fast and slow birefringence axes can be described by using the formalism of the differential matrix $\|N\|$ [10]. The change in the components of the electric field vector $\boldsymbol{E}$ of the wave in the basis of linear polarisation has the form

$$\left\| \begin{matrix} \mathrm{d}E_x/\mathrm{d}z \\ \mathrm{d}E_y/\mathrm{d}z \end{matrix} \right\| = \|N(z)\| \left\| \begin{matrix} E_x(z) \\ E_y(z) \end{matrix} \right\|. \tag{1}$$

The matrix $\|N\|$ describes the evolution of the electric vector of a plane light wave during the displacement of its wave front by a small distance $\mathrm{d}z$ along the propagation direction. By integrating Eqn (1), we obtain the complete Jones matrix $\|T\|$ determining the vector $\boldsymbol{E}(z)$ at the point z on the fibre axis from the known vector $\boldsymbol{E}(z=0)$:

$$\left\| \begin{matrix} E_x(z) \\ E_y(z) \end{matrix} \right\| = \|T(z)\| \left\| \begin{matrix} E_x(0) \\ E_y(0) \end{matrix} \right\|. \tag{2}$$

Below, all the matrices are represented in the basis of circular polarisations, which is more convenient for the interpretation of experiments.

A light wave propagating along the fibre experiences the linear birefringence with the coefficient $\Delta\beta = 2\pi/L_\mathrm{b}$, which is inherent in the fibre preform and is caused by the anisotropy of elastic tensions or by the core geometry; the circular birefringence with the coefficient $\gamma = 2\pi/L_\mathrm{F}$ caused by the Faraday effect; and the linear birefringence with the coefficient $\delta = 2\pi/L_\mathrm{ind}$ induced by the fibre winding on a spool of radius R (where L_b, L_F, and L_ind are the beat lengths of the corresponding birefringences) [11]. Let us emphasise that, in our opinion, the rotation of the preform causes only the rotation of axes (with the spatial frequency $\xi = 2\pi/L_\mathrm{tw}$, where L_tw is a step of the spial structure) of the linear birefringence. These types of birefringence and their differential matrices are presented in Table 1.

We measured in experiments the phase difference $\Delta\varphi = \delta_\mathrm{L} - \delta_\mathrm{R}$ between the left- and right-hand polarisation modes; therefore, a signal detected in our measurements is the additional phase difference $\Delta\varphi_\mathrm{F} = \Delta\varphi(\gamma) - \Delta\varphi(\gamma = 0)$ appearing after magnetic field switching.

2.1 Linear Spun fibre

The matrix $\|N\|$ for a linear Spun fibre in a longitudinal magnetic field has the form (Table 1)

$$\left\|N_\mathrm{cir}^\mathrm{Spun}\right\| = \left\| \begin{matrix} \mathrm{i}\gamma & \mathrm{i}(\Delta\beta/2)\exp(\mathrm{i}2\xi z) \\ \mathrm{i}(\Delta\beta/2)\exp(-\mathrm{i}2\xi z) & -\mathrm{i}\gamma \end{matrix} \right\|. \tag{3}$$

By integrating Eqns (1) with matrix (3), we obtain the complete Jones matrix

$$\left\|T_\mathrm{cir}^\mathrm{Spun}\right\| = \tag{4}$$

$$\left\| \begin{matrix} [\Omega\cos\Omega z - \mathrm{i}(\xi+\gamma)\sin\Omega z]\exp(\mathrm{i}\xi z) & \mathrm{i}(\Delta\beta/2)\sin\Omega z\exp(\mathrm{i}\xi z) \\ \mathrm{i}(\Delta\beta/2)\sin\Omega z\exp(-\mathrm{i}\xi z) & [\Omega\cos\Omega z + \mathrm{i}(\xi+\gamma)\sin\Omega z]\exp(-\mathrm{i}\xi z) \end{matrix} \right\|,$$

where

$$\Omega = \left[\Delta\beta^2/4 + (\xi+\gamma)^2\right]^{1/2} \tag{5}$$

is the spatial frequency. From matrix (4), we obtain a signal in the form of the phase delay

$$\begin{aligned} \Delta\varphi = \arctan\Bigg\{\Bigg[&\sin[2(\Omega-\xi)z] + \frac{(\Delta\beta/2)^2}{[\Omega+(\xi+\gamma)]^2} \\ &\times \sin[2(\Omega+\xi)z] - 2\,\frac{(\Delta\beta/2)^2}{(\xi+\gamma)[\Omega+(\xi+\gamma)]}\sin(2\xi z)\Bigg] \\ &\times\Bigg[\cos[2(\Omega-\xi)z] - \frac{(\Delta\beta/2)^2}{[\Omega+(\xi+\gamma)]^2}\cos[2(\Omega+\xi)z] \\ &- 2\,\frac{(\Delta\beta/2)^2}{(\xi+\gamma)[\Omega+(\xi+\gamma)]}\cos(2\xi z)\Bigg]^{-1}\Bigg\}. \end{aligned} \tag{6}$$

The expression in braces describes the complex beats of three spatial frequencies $\omega_1 = 2(\Omega-\xi)$, $\omega_2 = 2(\Omega+\xi)$, and $\omega_3 = 2\xi$ with different weights determined by the coefficients at sines and cosines. For $\Delta\beta \ll \xi$ (twisting dominates over linear birefringence), the signal is realised, as in the ideal case, in the form of the phase delay

$$\Delta\varphi_\mathrm{F} = 2\left\{\left[(\xi+\gamma)^2 + (\Delta\beta/2)^2\right]^{1/2} - \xi\right\}z \approx 2\gamma z$$

increasing with the fibre length.

For $\Delta\beta \gg \xi$, i.e., in the absence of twisting, the Spun fibre transforms to the HiBi fibre. By substituting $\xi = 0$ into (6), we can see that HiBi fibres are inconvenient for observing the Faraday effect because the signal accumulation with increasing the fibre length ceases at lengths $z > L_\mathrm{b}$.

Let us find the period z_{ω_1} of the spatial frequency ω_1 by substituting into (5) the expressions for $\Delta\beta$ and γ from

Table 1. Birefringence types and their differential matrices.

Birefringence type	Birefringence coefficient [11]	Differential matrix
Initial linear birefringence	$\Delta\beta = \dfrac{2\pi}{L_\mathrm{b}} = C_\mathrm{b} f(a,b)\dfrac{n_0^3(\lambda)}{\lambda}$	$\left\| \begin{matrix} 0 & \mathrm{i}(\Delta\beta/2) \\ \mathrm{i}(\Delta\beta/2) & 0 \end{matrix} \right\|$
Linear birefringence produced by winding	$\delta = \dfrac{2\pi}{L_\mathrm{ind}},\quad L_\mathrm{ind} = 22.792\,\dfrac{\lambda}{n_0^3(\lambda)}\,\dfrac{R^2}{r^2}$	$\left\| \begin{matrix} 0 & \mathrm{i}(\delta/2) \\ \mathrm{i}(\delta/2) & 0 \end{matrix} \right\|$
Circular birefringence induced by the Faraday effect	$\gamma = VB_z = \dfrac{2\pi}{L_\mathrm{F}},\quad V = \dfrac{8.13\times10^5}{\lambda^2-\lambda_V^2}$	$\left\| \begin{matrix} \mathrm{i}\gamma & 0 \\ 0 & -\mathrm{i}\gamma \end{matrix} \right\|$
Spiral structure	–	$\left\| \begin{matrix} 0 & \mathrm{i}(\Delta\beta/2)\exp(\mathrm{i}2\xi z) \\ \mathrm{i}(\Delta\beta/2)\exp(-\mathrm{i}2\xi z) & 0 \end{matrix} \right\|$

Note: n_0 is the average refractive index of the fibre; $f(a,b)$ is the fibre shape function; C_b is a constant depending on the elastic and thermodynamic properties of the fibre material; λ is the wavelength in nm; $\lambda_V = 118$ nm is the boundary wavelength; r is the external radius of the fibre.

Table 1 and $\xi = 2\pi/L_{tw}$. Taking into account that $L_F \gg L_b$, L_{tw}, we obtain

$$z_{\omega_1} = \frac{L_b L_{tw}}{\left(4L_b^2 + L_{tw}^2\right)^{1/2} - 2L_b}.$$

The expression for the period z_{ω_1} is similar to the relation for 'the beat length of the elliptic state' [1], which was obtained from a substantially different model. Note that z_{ω_1} is not the beat length of the polarisation eigenstate of Spun fibres, which depends on the length z of such fibres [even in the absence of a magnetic field ($\gamma = 0$)]. The period z_{ω_1} is only the beat length of the lowest of the three spatial frequencies dominating in the signal when $L_{tw} \ll L_b$.

2.2 Spun fibre wound on a spool

The differential matrix of a Spun fibre wound on a spool of radius R and placed in the magnetic field of a current has the form

$$\left\| N_{cir}^{Spun+} \right\| = \tag{7}$$

$$\left\| \begin{matrix} i\gamma & i(\Delta\beta/2)\exp(i2\xi z) + i(\delta/2) \\ i(\Delta\beta/2)\exp(-i2\xi z) + i(\delta/2) & -i\gamma \end{matrix} \right\|.$$

The solution of Eqns (1) with matrix (7) leads to the Riccati equation with coefficients of the type of the matrix element N_{12}, which has no standard solutions.

Then, the calculation was performed numerically. According to (1), taking matrix (7) into account, we obtain the expressions for the electric fields with the left- and right-hand circular polarisations:

$$\begin{aligned} \frac{dE_L}{dz} &= -i\gamma E_L + i[(\Delta\beta/2)\exp(i2\xi z) + (\delta/2)]E_R, \\ \frac{dE_R}{dz} &= i[(\Delta\beta/2)\exp(-i2\xi z) + (\delta/2)]E_L + i\gamma E_R. \end{aligned} \tag{8}$$

By integrating numerically (8), we calculated the dependence $\Delta\varphi_F(z)$ for the contour diameters $D = 77.4$, 44.7, and 20 mm to which the beat lengths $L_{ind} = 4500$, 1500, and 300 mm of the induced birefringence correspond. The evolution of the signal along the fibre axis of length 16 m at the last 100 cm is shown in Fig. 1. The fibre parameters were $L_{tw} = 2$ mm, $L_b = 15$ mm, and $J = 3$ A (recall that the magnetic field of current along the fibre axis is proportional to $1/D$). The thin lines in Fig. 1 correspond to the case when all the types of birefringence except for the Faraday type are absent in the fibre (ideal signal). It follows from Fig. 1a that the output signal contains beats between the high-frequency components ω_2 and ω_3 and has the envelope with a period equal to 445 mm for $D = 44.7$ mm. We assumed that this period corresponds to the frequency ω_1 from expression (6). Indeed, the estimate of the period of frequency ω_1 gives $z_{\omega_1} \approx 4L_b^2/L_{tw} \approx 450$ mm. Thus, the birefringence induced by the fibre bending does not give rise to new frequencies in the signal $\Delta\varphi$; however, the frequency $\omega_3 = 2\xi$ spreads to the spectrum of width $\Delta\xi \approx 4\xi(\delta/\Delta\beta)$, which causes the nonharmonic behaviour of the signal envelope up to $L_{ind}/L_b \sim 100$. One can see from Fig. 1b that the envelope resembles a sinusoid only for $L_{ind}/L_b \sim 300$.

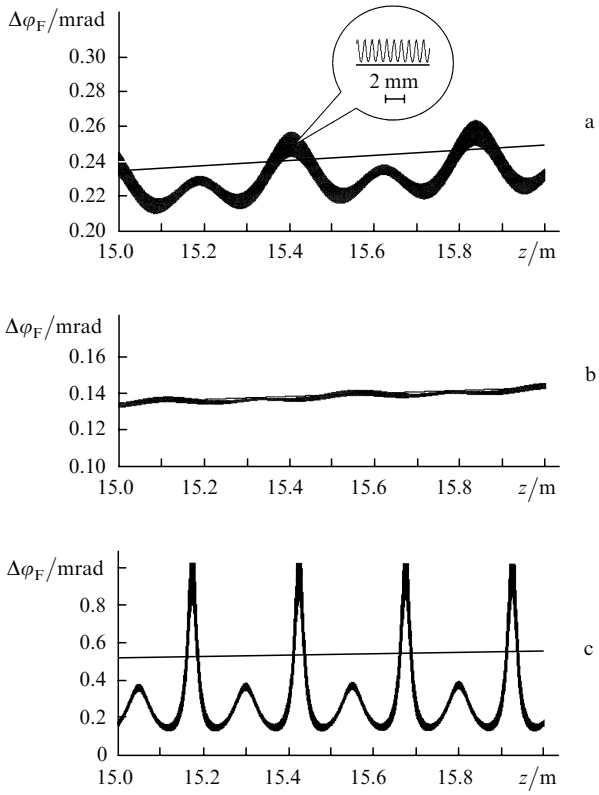

Figure 1. Evolution of a signal over the last 100 cm of the Spun fibre length (the total fibre length is $L = 16$ m) for the winding diameters $D = 44.7$ (a), 77.4 (b), and 20 mm (c). The thin lines correspond to the ideal signal.

Consider the effect of a radiation source on the signal. The refractive-index dispersion $dn/d\lambda = 1.23 \times 10^{-5}$ nm^{-1} at $\lambda = 1550$ nm results in the wavelength dependence of the coefficients $\Delta\beta$ and δ of the linear birefringence. For the circular birefringence caused by the Faraday effect, the wavelength dependence is determined by the Verdet constant [12] (Table 1). The calculation of the evolution of signals in the vicinity of $\lambda = 1550$ nm, whose wavelength differed by $\Delta\lambda = 15$ nm, showed that these signals preserved their shape but shifted along the fibre axis by a distance of ~ 13 mm. This means that, by using a light source with the spectral width 15 nm, we obtain a signal averaged over the interval $\Delta z \sim 13$ mm. It is clear that such a signal will not contain both high-frequency spatial components ω_2 and ω_3 (for this, averaging over the interval $\Delta z \sim 2.5$ mm is sufficient), and a periodic function at the frequency ω_1 will be partially smoothed (Fig. 2).

By comparing the calculations with experiment data, it is also necessary to take into account other reasons for signal

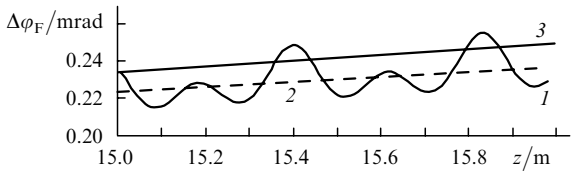

Figure 2. Evolution of a signal (*1*), similar to that in Fig. 1a, after averaging for $\Delta z = 13$ mm. Curve (*2*) is the averaging for $\Delta z = 107$ mm, curve (*3*) is the ideal signal.

averaging. Thus, the ellipticity of a spool, variations in the beat length in the fibre or in the step of the spiral structure of the order of 1 % result in averaging over the intervals $\Delta z \sim 11$, ~ 20, and ~ 7 mm, respectively. Our analysis showed that the strongest averaging ($\Delta z \sim 107$ mm) is caused by the delayed phase modulation, resulting in the absence of oscillations of the signal [curve (*2*) in Fig. 2].

We calculated the sensitivity of the sensor normalised to its sensitivity upon detecting an ideal signal (provided by a fibre in which all the types of birefringence are absent except for birefringence induced by the magnetic field of an electrical current) for different winding diameters of the Spun fibre.

3. Experiment

We developed a FOCS in which the electric current is measured by the phase method. This sensor was used as a tool to verify the proposed model of a Spun fibre. The block diagram of the FOCS is shown in Fig. 3. The optical part of the sensor is an all-fibre low-coherence linear interferometer similar to that described in [2, 3]. Radiation source (*1*) is a diode-pumped erbium-doped silica fibre superluminescence source emitting ~ 10 mW at 1550 nm. The width of the emission spectrum was 15 nm.

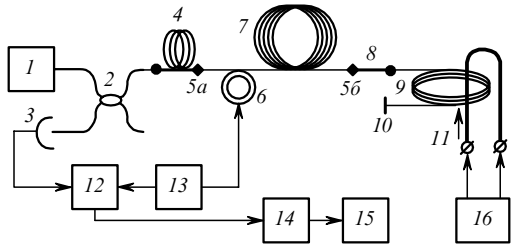

Figure 3. Block diagram of the FOCS: (*1*) light source; (*2*) directional coupler; (*3*) photodetector; (*4*) polariser; (*5a*, *5b*) 45° fibre splicings; (*6*) birefringence modulator; (*7*) fibre line; (*8*) quater-wave plate; (*9*) sensitive contour; (*10*) mirror; (*11*) wire with flowing current; (*12*) phase detector; (*13*) reference generator; (*14*) ADC; (*15*) computer; (*16*) current source.

Optical radiation passes through directional coupler (*2*) and fibre polariser (*4*) and is coupled to fibre birefringence modulator (*6*), the transmission axis of the polariser being oriented [splicing (*5a*)] at an angle of 45° to the birefringence axes of the input fibre of the modulator. In the fibre of the modulator [beginning from splicing (*5a*)], radiation propagates in the form of two light waves of equal intensities with orthogonal linear polarisations. The modulator is made of a PANDA fibre wound on a piezoelectric cylinder of diameter 30 mm with the tension 50 g. Then, the radiation passes through PANDA fibre line (*7*) of length 900 m and quarter-wave phase plate (*8*) whose axes are oriented at an angle of 45° to the axes of fibre line (*7*) [splicing (*5b*)]. The phase plate is made of a PANDA fibre (the beat length is 4 mm).

The orthogonal circularly polarised waves formed by the phase plate propagate in sensitive Spun fibre contour (*9*) ($L_b = 15$ mm, $L_{tw} = 2$ mm) of length $L = 16$ m. After reflection from mirror (*10*), these modes, having changed the direction of circular polarisation to the opposite, propagate in the opposite direction. After the second passage through phase plate (*8*), the circularly polarised modes are again transformed to linearly polarised modes, the x mode being transformed to the y mode, and vice versa. As a result, all the phase shifts between polarised modes caused by reciprocal effects (the influence of the refractive index of the medium and birefringence in the fibre) are compensated at the input of polariser (*4*) [splicing (*5a*)], and only the Faraday phase shift $\Delta\varphi_F$ related to the electric current being measured is preserved.

The components of both linearly polarised modes collinear to the transmission axis of the polariser pass through the polariser and interfere. Then, the interference signal is directed through coupler (*2*) to photodetector (*3*). The Faraday phase shift $\Delta\varphi_F$ is recorded by the modulation method, which is widely used in fibreoptic gyroscopes and is based on the delayed harmonic modulation of the phase shift between the working light waves of the interferometer [13].

The modulation is performed with the help of birefringence modulator (*6*). The time delay between the input and output light waves required to increase the phase modulation efficiency is provided by using fibre line (*7*). The modulator is excited by generator (*13*) operating at the frequency $f_m = 40$ kHz and provides the modulation $\varphi_m(t) = \Psi_m \cos(2\pi f_m t)$ of the phase shift between the x and y modes with the amplitude $\Psi_m = 1.2$ rad. The radiation power P incident on photodetector (*3*) (assuming that $\varphi_m(t)$, $\Delta\varphi_F \ll 1$) can be written in the form

$$P \approx \frac{P_0}{2}\left[1 + 2\Delta\varphi_F \Psi_m \cos(2\pi f_m t) + \frac{\Psi_m^2}{2}\cos^2(2\pi f_m t)\right].$$

The output voltage of phase detector (*12*) tuned to the separation of a signal proportional to $\cos(2\pi f_m t)$ is proportional to the phase shift caused by the Faraday effect: $U_0 = \kappa\Delta\varphi_F$, $\kappa = \text{const}$. The output signal of the phase detector is digitised in ADC (*14*) and is recorded in computer (*15*). The current measured in conductor (*11*) is controlled by current stabiliser (*16*).

Figure 4 presents the output characteristic of the FOCS. The fibre spool of the sensitive contour used in the sensor was located inside a toroidal winding consisting of 370 copper wire coils. This construction provided a magnetic field equivalent to an electric current that was 370 times higher than that provided by current stabiliser (*16*). The maximum measured equivalent current was 3000 A.

The minimum current was determined by the FOCS threshold sensitivity equal to 70 mA $Hz^{-1/2}$ (the intrinsic

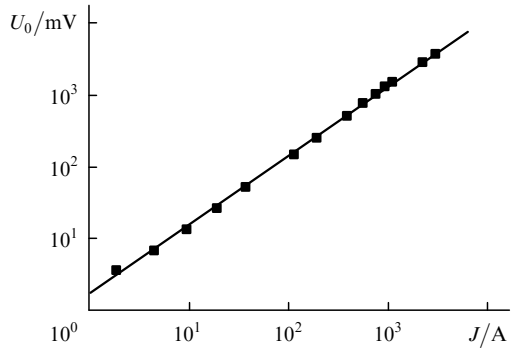

Figure 4. Output characteristic of the FOCS ($D = 155$ mm, $N_0 = 27$).

noise of the sensor was ~ 0.5 mV). The FOCS sensitivity was $k_1 = \mathrm{d}U_0/\mathrm{d}J = 6.4$ mV A^{-1}. The output signal instability was less than 0.1 % for two hours. The sensitivity error did not exceed 0.6 % for 22 days (the confidence region was 1σ). We measured the sensitivity of FOCS by winding Spun fibres on spools with different diameters D. The sensitivity k_2 per contour coil ($k_2 = k_1/N_0$) expressed in mV A^{-1} coil^{-1} was also measured. Figure 5 shows the experimental dependences $k_2(L)$ for different D. The dependence of the sensitivity on the diameter D is shown in Fig. 6 (points).

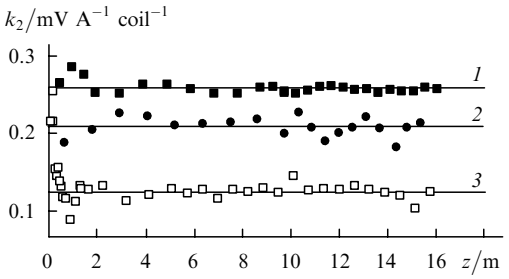

Figure 5. Experimental dependences of the FOCS sensitivity on the length z of the Spun fibre wound on a spool. The total length of the fibre is $L = 16$ m and the winding diameter is $D = 155$ (*1*), 36 (*2*), and 20 mm (*3*).

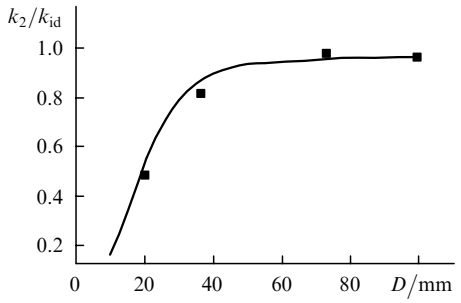

Figure 6. Sensitivity of the sensor normalised to its sensitivity upon detecting the ideal signal as a function of the winding diameter D of the Spun fibre (curve: theory, points: experiment).

4. Discussion of results

In experiments with contours of different diameters (Fig. 5), we obtained constant values of the sensitivity k_2 per coil [or the slope of the signal accumulation function (Fig. 2)], which were independent of the fibre length at least up to 16 m. The deviation from such behaviour is expected only for fibre lengths of the order of the beat length $L_F \sim 10^5$ m. As the contour diameter is decreased ($D <$ 70 mm), the sensitivity k_2 decreases (Fig. 6), in good agreement with the theory. Note that this decrease occurs when the internal linear birefringence of the Spun fibre exceeds the linear birefringence produced by winding. Thus, $k_2/k_{id} = 0.2$ for $L_{ind}/L_b \sim 10$ and $D = 14$ mm, where k_{id} is the sensitivity of a fibre which has only the Faraday birefringence.

Let us turn to Fig. 5. Small variations in the sensitivity k_2 over the fibre length can be explained by the modulation of the signal at the spatial frequency ω_1 due to incomplete averaging. Because the winding length was changed by an integer number of coil lengths, the dependences in Fig. 5 have the character of a random sampling.

5. Conclusions

We have studied the polarisation properties of Spun fibres from the point of view of their application in current sensors based on the Faraday effect. The study was performed by using the FOCS developed by us. The sensor is based on a low-coherence linear reflection interferometer with a threshold sensitivity of 70 mA Hz$^{-1/2}$, a maximum measured current of 3000 A, and a scale-factor reproducibility of ± 0.6 %.

The properties of Spun fibres have been interpreted by using the theory developed in the paper, which is based on the concept of the spiral structure of the linear birefringence axes produced during fibre drawing from a rotating preform. The method of integration of the differential Jones matrix has been used. For a linear Spun fibre in a magnetic field, the solution has been obtained in quadratures, while for a Spun fibre wound on a spool the differential matrix was integrated numerically.

Our calculations have shown that in the Spun fibre wound on a spool, the linear birefringence induced by the elastic bending (with the radius R) of the fibre is partially compensated, which determines the advantage of fibres of this type as sensitive elements in the current sensors based on the Faraday effect. However, for a comparatively weak condition $L_{tw} < L_b$, a more rigid condition $20L_b < L_{ind}$ should be satisfied.

The results of measurements of the sensor sensitivity as a function of the spool diameter and winding length confirmed the theoretical conclusions. In particular, it has been shown experimentally that for a given contour diameter, the average sensitivity per coil for $L \leqslant 16$ m is almost independent of the fibre length. The reduction of the sensitivity with decreasing the winding diameter coincides with the theoretical calculation.

References

1. Laming R.I., Payne D.N. *J. Lightwave Technol.*, **7**, 2084 (1989).
2. Blake J., Tantaswadi P., de Carvalho. *IEEE Trans. on Power Delivery*, **11**, 116 (1996).
3. Bohnert K., Gabus P., Nehring J., Brändle H. *J. Lightwave Technol.*, **20**, 267 (2002).
4. Takahashi M. et al. *IEEE Trans. on Power Delivery*, **12**, 1422 (1997).
5. Bosselmann T. *Proc. Conf. OFS-9* (Firenze, Italia, 1993) p. 297.
6. Rose A.H., Polinkin P.G., Blake J. *Proc. Conf. OFS-14* (Venice, Italia, 2000) TH3-5.
7. Aksenov V.A., Ivanov G.A., Morshnev S.K., Chamorovskii Yu.K. *13-ya Mezhdunarodnaya nauchnaya konferentsiya MMTT-2000* (13 International Conference MMTT-2000) (St. Petersburg, 2000) Vol. 7, section 10, p. 53.
8. Aksenov V.A., Voloshin V.V., Vorob'ev I.L., Ivanov G.A., Isaev V.A., Kolosovskii A.O., Morshnev S.K., Chamorovskii Yu.K. *Radiotekh. Elektron.*, **47**, 1011 (2002).
9. Barlow A.J., Ramskov-Hansen J.J., Payne D.N. *Appl. Opt.*, **20**, 2962 (1981).
10. Azzam R.M.A., Bashara N.M. *Ellipsometry and Polarised Light* (Amsterdam – New York – Oxford: North-Holland Publ. Comp., 1977).
11. Rashleigh S.C. *J. Lightwave Technol.*, **1**, 312 (1983).
12. Robinson C.C. *Appl. Opt.*, **3**, 1163 (1964).
13. Berg R.A., Lefevre H.C., Show H.J. *J. Lightwave Technol.*, **2**, 91 (1984).